Geophysical Research Letters

Key Points:
- A better resolution of the tectonic events and plate interface geometry beneath the southernmost Ryukyu arc and forearc
- Tectonic exhumation occurs in the frontal portion of the southernmost Ryukyu seismogenic zone
- Tectonic underplating occurs beneath the southernmost Ryukyu seismogenic zone

Earthquake-Related Structures Beneath the Southernmost Portion of the Ryukyu Arc and Forearc

Shiou-Ya Wang[1] ⓘD, Shu-Kun Hsu[1,2] ⓘD, and Yi-Ching Yeh[1]

[1]Department of Earth Sciences, National Central University, Taiwan, [2]Center for Environmental Studies, National central University, Taiwan

Abstract Moderate to large earthquakes repeatedly occur beneath the southernmost Ryukyu arc and forearc, but the seismogenic structures were poorly studied. To better understand the southernmost Ryukyu seismogenic structures, we have deployed ocean bottom seismometers to record the aftershocks of a large earthquake in 2015. As a result, several groups of aftershocks are associated with the seismogenic structures. A deep group coincides with the north-dipping seismogenic zone that terminates near the tip of the mantle wedge beneath the Ryukyu Arc. A shallow group dips southward from the southern slope of the Ryukyu Arc to the southern end of the aftershocks; this group shows south-dipping normal faulting character and accompanies the lower crust exhumation of Ryukyu Arc above the seismogenic zone. A plate interface step-down beneath the seismogenic zone is inferred. A crustal underplating and exhumation around the seismogenic zone have taken place synchronously during the earthquake event.

Plain Language Summary Large earthquakes frequently occur at the plate boundary where two plates converge. Those earthquakes usually appear at a segment of the downgoing plate surface, called a seismogenic zone. Seismogenic zones are extensively studied in order to understand the possible earthquake cycles, crustal stress variation, mechanisms of earthquake nucleation, rupture propagation, and so on. Historically, the southernmost Ryukyu seismogenic zone has generated numerous earthquakes but its seismogenic structures are still unclear. By studying aftershocks of a large earthquake in 2015, we show the general characters of the southernmost Ryukyu seismogenic zone and indicate a synchronous occurrence of the uplift of the south Ryukyu Arc and accumulation of some subducted material beneath the Ryukyu Arc.

1. Introduction

Subducting plate interfaces can produce the world's largest earthquakes through thrust faulting. Studying the seismogenic zone features of subduction zones is thus important to understand mechanisms of generating megathrust earthquakes along the subducting plate interfaces. Previous studies of subduction zones mostly reveal the features related to the updip and downdip limits of seismogenic zones (Almeida et al., 2018; Herrendörfer et al., 2015; Hsu et al., 2006; Hyndman et al., 1997; Hyndman, 2013; Kinoshita et al., 2017; Moore & Saffer, 2001; Wang & Hu, 2006). Particularly, megathrust earthquakes could be controlled by the downdip widths of the seismogenic zones (Herrendörfer et al., 2015). On the other hand, an active underplating or peeling off the uppermost part of a subducting material and accretion to the bottom of an overriding plate could take place around seismogenic zones (Kimura et al., 2010). Accretion of oceanic crust to the continent in subduction zones may be found at either the toe of an accretionary prism or at a deep part of a subduction zone (Matsumura et al., 2003).

Unlike other subduction zones, the seismogenic zone-related features in the south Ryukyu subduction zone were poorly understood. In the southernmost Ryukyu subduction zone, a cluster of repeated moderate to large earthquakes exists beneath the Nanao (forearc) Basin along the subducting plate interface (e.g., Kao et al., 1998; Lallemand et al., 2013; Figure 1). More than 10 earthquakes with magnitude greater than 7 have been recorded since the beginning of the last century, including the historically largest earthquake of Mw 7.7 earthquake in 1920 (Theunissen et al., 2010). Nevertheless, detailed earthquake observations in the southernmost Ryukyu subduction zone are insufficient because of the poor azimuthal coverage or the far distance from the onshore seismic network.
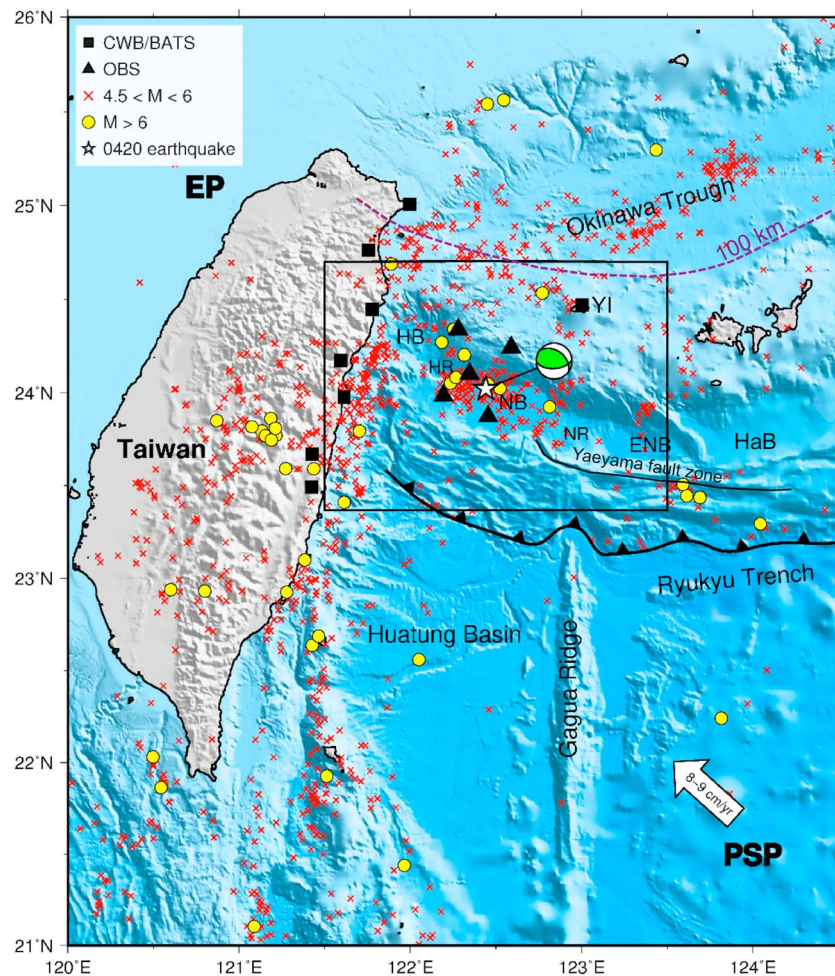
Figure 1. Topography and major earthquakes around the south Ryukyu subduction zone from 1995 to 2016. The white star and the focal mechanism in gray indicate the main shock of 0420 event on 20 April 2015. The black triangles indicate the deployed OBSs that have recorded the aftershocks. The black squares are the onshore seismic stations used together with the OBSs. ENB = East Nanao Basin; EP = Eurasian Plate; HaB = Hateruma Basin; HB = Hoping Basin; HR = Hoping Rise; NB = Nanao Basin; NR = Nanao Rise; PSP = Philippine Sea Plate; YI = Yonaguni Island. The white arrow indicates the PSP plate motion relative to EP. The purple dashed line indicates the contour line of subducted slab of 100 km deep. CWB = Central Weather Bureau; OBS = Ocean Bottom Seismometer.

On 20 April 2015, an earthquake with a magnitude of M_L 6.1 and the epicentral depth of ~25 km occurred beneath the Nanao Basin (see Table S1 in the supporting information; hereafter referred to as the 0420 event; Figure 1). The 0420 event provides us with a good opportunity to better understand the complex tectonics of the southernmost Ryukyu seismogenic zone. Thus, we have deployed an Ocean Bottom Seismometer (OBS) array around the Nanao Basin (Figure 1) to record the aftershocks. In this paper, we show the tectonic structures associated with the 0420 event and discuss the seismogenic zone-related features of the southernmost Ryukyu subduction zone.

2. Tectonic Background

2.1. South Ryukyu Arc and Forearc

Located between the Philippine Sea Plate (PSP) and the Eurasian Plate, the Ryukyu subduction zone extends from the Kyushu Island of Japan in the northeast to the Taiwan Island in the southwest. Morphologically, it displays a typical arc-shaped trench-arc-backarc system. The PSP has subducted northwestward beneath the Eurasian Plate along the Ryukyu Trench in a speed of ~ 80–90 mm/year near the Taiwan-Ryukyu junction area (Seno et al., 1993; Yu et al., 1997; Figure 1). However, the current south Ryukyu arc is nonvolcanic; the
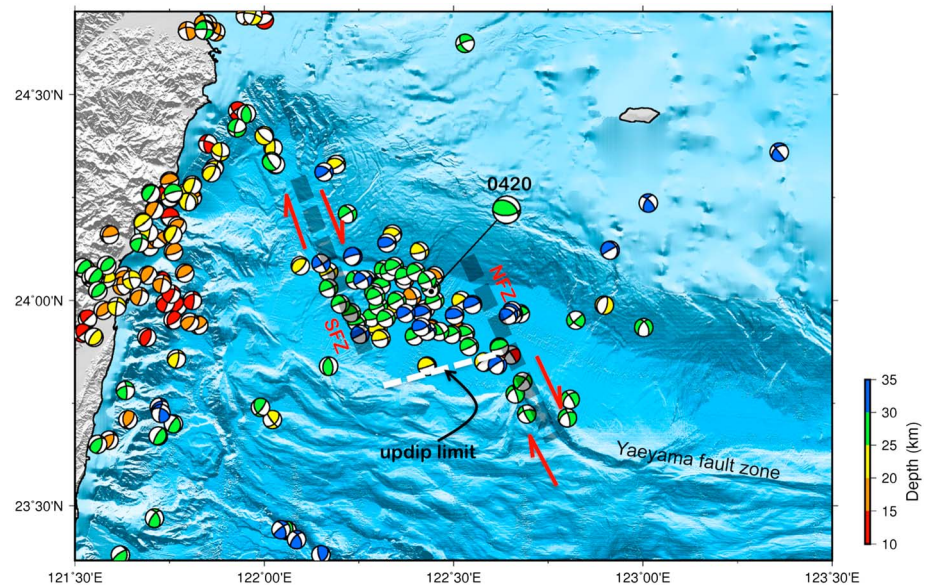
Figure 2. The focal mechanisms of crustal earthquakes with magnitudes greater than 4.5 from 1995 to 2016 from BATS (http://bats.earth.sinica.edu.tw). It is noted that the earthquakes cluster beneath the western portion of the Nanao Basin. The focal mechanism with label 0420 indicates the main shock of 0420 event. SFZ = Suao Fault Zone; NFZ = Nanao Fault Zone.

volcanic front (contour line of the subducted slab at 100 km deep) is along the southern margin of the Okinawa Trough backarc basin (Hsu et al., 2001; Figure 1). The Taiwan-Ryukyu junction area is also a transition zone from the PSP collision in the west to PSP subduction in the north (Angelier, 1990; Ho, 1986; Lallemand et al., 2013; Sibuet & Hsu, 2004; Suppe, 1984; Teng, 1990). Probably because of the collision/subduction transition, the fast retreating of the south Ryukyu Arc (Hsu, 2001), and the clockwise rotation of the south Ryukyu Arc (Chen et al., 2018; Nishimura et al., 2004), the Ryukyu arc-trench system changes its orientation near 123°E from W-E to NW-SE, parallel to the plate convergence direction (Figure 1).

Along ~123°E, the Gagua Ridge is ~300 km long, ~30 km wide, and ~4 km high above the seafloor (Font et al., 2001). The Gagua Ridge could be a transverse ridge (Hsu et al., 1998) and is a linear feature in northwest PSP. The northwestward subduction of the N-S trending Gagua Ridge could affect the morphology and structures of the south Ryukyu forearc (Dominguez et al., 1998; Figure 1). The south Ryukyu accretionary prism has thus been indented and part of the forearc basins has been uplifted (Dominguez et al., 1998). To the east of 123°E, the oblique subduction has caused an obvious strain partitioning and created the roughly W-E trending Yaeyama Fault Zone inside the accretionary prism (Dominguez et al., 1998; Lallemand et al., 1999; Figure 1). To the west of 123°E, the Yaeyama Fault Zone changes its orientation to NW-SE direction (Figure 1); this change could reflect the right-lateral strike-slip faults in the northwest area above the subducted Gagua Ridge (Dominguez et al., 1998) and/or a NW-SE trending faulting across the south Ryukyu Arc and forearc (Hsu et al., 1996). The NW-SE trending faulting is coherent with the historically right-lateral strike-slip focal mechanisms as shown in Figure 2. To differentiate the NW-SE trending fault zone across the forearc from the W-E trending segment of the Yaeyama Fault Zone that is due to a strain partitioning, we name it the Nanao Fault Zone (NFZ). The NFZ marks the eastern boundary of the Nanao cluster (Figure 2).

2.2. Seismicity

Here we call the Nanao cluster because moderate to large earthquakes have clustered beneath the Nanao Basin of the southernmost Ryukyu subduction zone (Figures 1 and 2). In addition to the NFZ in the east side of the Nanao cluster, we also observe right-lateral strike-slip focal mechanisms in the west side of the Nanao cluster (Figure 2). We may infer a NW-SE trending right-lateral Suao Fault Zone (SFZ) in the western boundary of the Nanao cluster (Figure 2). Although there are still some components of shearing for the
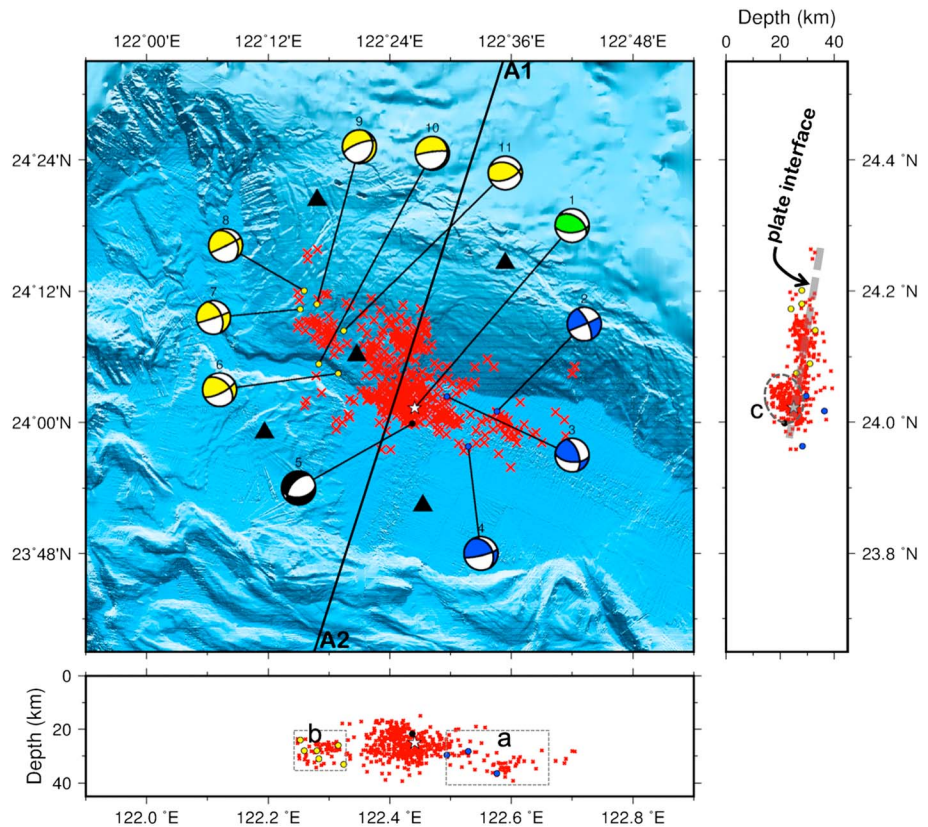
Figure 3. The distribution of the 14-day aftershocks of 0420 event. Note that the earthquakes generally display a NW-SE trend and can be divided into several groups. The deeper group generally follows the seismogenic zone of the subducting plate interface, suggested by the seismic refraction study of T. K. Wang et al. (2004) and the tomographic study of Lallemand et al. (2013). The detailed information of the focal mechanisms in numbers is shown in Table S1.

earthquakes inside the Nanao cluster, the earthquakes inside the Nanao cluster mainly exhibit thrusting mechanism (Figure 2). Two multichannel seismic reflection profiles across the Nanao Basin show that active shearing faults mainly exist along the NFZ and SFZ (Figure S1).

The abundant seismicity of the Nanao cluster could be due to an additional stress on the subducting plate interface in a restraining overstep between the *en échelon* dextral strike-slip SFZ and the NFZ (Figure 2). The moderate to large earthquakes with low-angle thrust mechanism beneath the Nanao Basin mainly occurred at the seismogenic zone of the subducting plate interface (Kao et al., 1998). Based on the earthquake report of the Central Weather Bureau of Taiwan, the main shock of 0420 event is inside the Nanao cluster (Figure 2).

3. Data Acquisition and Processing

One day after the main shock of 0420 event, we have deployed six short-period OBSs surrounding the main shock and recorded the aftershock data from 21 April to 5 May 2016 (14 days); however, only five OBSs were successfully recovered (Figure 1). Each OBS contains one vertical and two horizontal seismometers, and one hydrophone. The distance between OBSs was between 20 and 45 km. In order to relocate all the OBSs, we have shot air-gun source above each OBS from 4 May to 5 May 2016. The final location of each OBS was inverted from the travel time of direct water wave by using least-square method. We used least-square method to find minimum residuals between the pick direct-wave arrival time and theoretical arrival time. The final OBS locations are shown in Figure 3. All the OBSs have recorded good quality data. To have a better coverage of the seismic wave azimuths and improve the earthquake location accuracy, we have also used earthquake data from eight broadband stations that are situated in eastern Taiwan from Central Weather

Bureau Seismic Network and one from Yonaguni Island of Japan Meteorological Agency (Shin et al., 2013; Figure 1).

We used the Short Term Averaging/Long Term Averaging ratio algorithm (Allen, 1978) to detect the *P* wave arrivals, then check the *P* wave quality and pick *S* wave arrival artificially. We extracted the events that were recorded by six stations or more. In total, over 700 events were detected, 631 events were initially located beneath the south Ryukyu forearc basins by using iasp91 model (Kennett & Engdahl, 1991).

In order to have a better result, we apply software VELEST (Kissling et al., 1995) and HypoDD (Waldhauser & Ellsworth, 2000) to relocated earthquakes. First, we compute the best-fit 1-D velocity model throughout the region by using the joint hypocenter-velocity model inversion software package VELEST. The initial 1-D Velocity model is based on Lallemand et al. (2013). The 4,088 *P* wave and 2,105 *S* wave arrival times of 601 events were inverted to estimate the best-fit 1-D velocity model. The average RMS residuals of final velocity model reduce from 0.70 to 0.24 s. To test the velocity model stability, we generated 1,000 random models ($\pm$5% of velocity perturbation applied to each layer of the initial velocity model) and repeated the inversion step. The RMS residuals of the 1,000 random models are between 0.23 and 0.38 s and the models with lower RMS (i.e., RMS residuals between 0.23 and 0.25 s) show a similar pattern with the inverted model of initial model. The results suggest the final velocity model is well constrained (Figure S2). Then, the inverted velocity model was used as the input model of HypoDD to further improve the earthquake locations. Relocation program HypoDD uses double-difference method, which takes the advantage that the distance between any two hypocenters of earthquake are much shorter than the distance to the event station. In other words, the double-difference method can minimize the error from velocity model. The detailed algorithm can be found in Waldhauser and Ellsworth (2000). HypoDD provides singular value decomposition (SVD) and conjugate gradient least-square (LSQR; Paige & Saunders, 1982) to solve the double-difference equations. SVD is applicable for small systems and provides error estimate, while LSQR is efficient for large systems. We only relocate earthquakes with at least five arrivals and 4 km is set for the separation of each event-pair. The entire earthquakes were relocated by LSQR. The location errors were calculated by using SVD for subsets of the catalog, because the errors may be underestimated by LSQR (Waldhauser & Ellsworth, 2000). The average errors of 2 standard deviation in horizontal and vertical distances are ~1.0 and ~1.6 km, respectively (Figure S3). In total, 511 earthquakes were relocated successfully. The distribution of the seismicity is shown in Figure 3.

To calculate the local magnitude (M_L) for all the aftershocks, we used a normalized attenuation function and the focal depths of earthquake in the Taiwan area (Shin, 1993). There are 78 earthquakes commonly recorded by both the inland permanent seismic stations and the OBS network; their magnitudes ranges from 1.2 to 5.6. Due to a limited coverage of our stations, only three focal mechanism solutions close to the NFZ were well determined by using *P* wave first motion method (the solutions in blue in Figure 3).

4. Results and Discussions

The relocated aftershocks of the 0420 event are generally distributed beneath the northwestern portion of the Nanao Basin and around the southern slope of the south Ryukyu Arc, generally inside the Nanao cluster (Figure 3). The aftershocks show a NW-SE trend with focal depths ranging between ~15 and ~40 km (Figure 3). The aftershocks can be divided into several groups (Figure 3).

4.1. Seismogenic Zone

Situated in the middle of the aftershocks, the first group of the aftershocks deepens northward and has the hypocentral depths ranging from ~24 to ~32 km. Following a cross-section roughly perpendicular to the trend of the southernmost Ryukyu Arc and the aftershocks (Profile A1-A2 in Figure 3) and superposed on the velocity model of Lallemand et al. (2013), most of the first group aftershocks occurred along the seismogenic zone of the subduction plate interface (Figure 4). Based on the distribution of historically moderate to large earthquakes in the Nanao Basin (Figure 2), we found the southernmost limit of the earthquakes is at ~20 km deep (Figures 2 and 4). Because those earthquakes display low-angle thrusts along the plate interface (Kao et al., 1998), we could infer that the updip limit of the seismogenic zone in the southernmost Ryukyu subduction zone is at ~20 km deep (Figures 2 and 4). In contrast to the updip limit beneath the fold-and-thrust zone of the accretionary prism in the Cascadia subduction zone (Hyndman, 2013), the updip limit
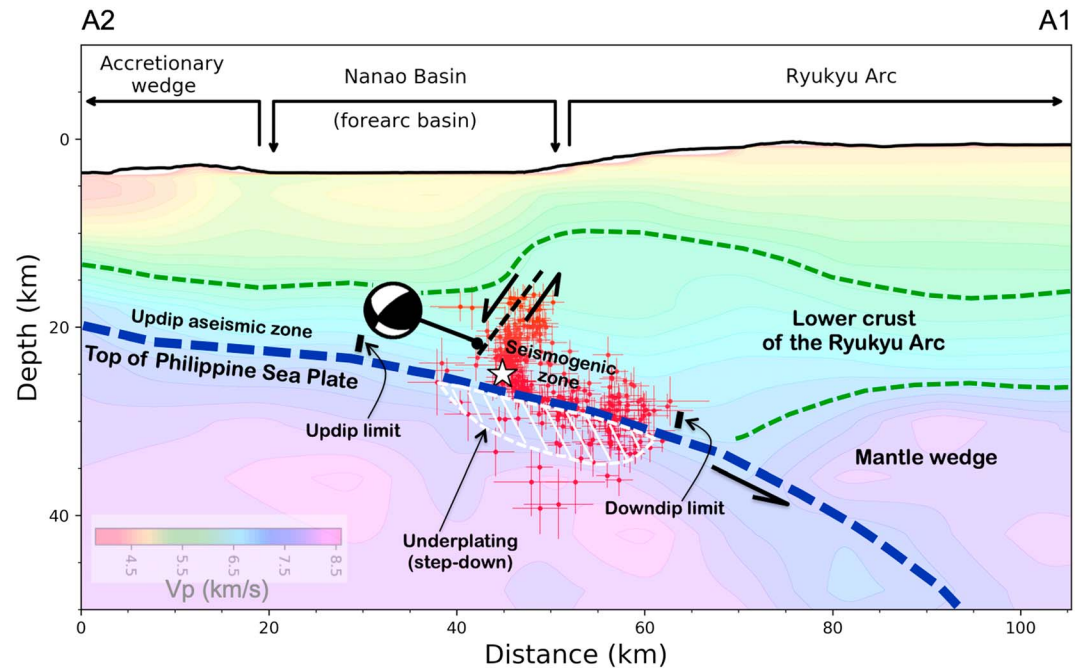
Figure 4. The aftershocks of 0420 event and the overall structures around the south Ryukyu seismogenic zone. Red crosses indicate 2 standard deviation error bars. Note that appearance of the step-down of the plate interface is close to the updip limit of the seismogenic zone and coincides with the bottom of the normal faulting earthquakes. It is also noted that the crust of the south Ryukyu Arc above the seismogenic zone has been exhumed. The two focal mechanisms are from Theunissen et al. (2012). The velocity structure is from Lallemand et al. (2013). The white star indicates the 0420 event main shock.

in the southernmost Ryukyu subduction system is located beneath the forearc basin. On the other hand, the downdip limit of the seismogenic zone terminates at ~32 km deep near the tip of the mantle wedge beneath the Ryukyu Arc (Figure 4). The downdip limit location of the south Ryukyu subduction zone agrees well with the observation in other subduction zones that the downdip limit generally terminates near the mantle wedge and is thermally controlled (Hyndman et al., 1997). The width of the southernmost Ryukyu seismogenic zone is estimated to be only ~35 km (Figure 4), which is much less than the global average of the seismogenic zone widths (Hayes et al., 2012; Heuret et al., 2011). A possible explanation for such a short width of the seismogenic zone is that the southernmost Okinawa Trough has a fast backarc opening. The southernmost Ryukyu Arc has a fast southward migration so that the volcanic front is situated in the southern margin of the Okinawa Trough, instead of the southernmost Ryukyu Arc.

4.2. Strike-Slip Faulting

There are two groups of the aftershocks distributed in the west and east sides of the aftershocks (inside rectangles a and b in Figure 3), respectively. The group a contains earthquakes with dextral strike-slip focal mechanisms determined from this study (Table S1). However, we are not able to determine any focal mechanism from the aftershocks inside group b. Based on the historical BATS focal mechanism solutions inside group b, group b probably contain both thrusting and dextral strike-slip components (Figure 3). It is noted that groups a and b mainly occurred in the deep portion, roughly along the seismogenic zone (Figure 3). The difference between these two groups is that group a is close to the frontal portion of the seismogenic zone, but group b is close to the rear portion of the seismogenic zone (Figure 3). That distribution is similar to the *en échelon* pattern of the SFZ and the NFZ (Figure 2). Because right-lateral strike-slip aftershock groups a and b are around the NFZ and the SFZ, respectively, we may suggest that the thrusting of 0420 main shock occurred in the contractional overstep between the SFZ and the NFZ (e.g., Kearey et al., 2009). This inference is consistent with the fault rupture of the 0420 main shock that was propagating southeastward and upward along the plate interface (Lee, 2015).

4.3. Underplating

The seismic velocity structure below the frontal portion of the seismogenic zone is relatively depressed (Lallemand et al., 2013; Figure 4). Lallemand et al. (2013) interpreted the depressed zone as a near-vertical sheared zone on the PSP. However, there are several aftershocks occurred beneath the seimogenic zone (Figure 4), we may interpret the low depressed area as the "step-down" of the subducting plate interface and an underplating beneath the southernmost Ryukyu seismogenic zone. It is similar to the underplating in the Naikai seismogenic zone (Kimura et al., 2007; Kimura et al., 2010; Kimura & Ludden, 1995; Matsumura et al., 2003). The focal mechanisms around the depressed velocity zone could be either inter-preted as a near-vertical fault planes or low angle thrusting fault planes parallel to the seismogenic zone. We prefer the latter because the southernmost Ryukyu Arc is uplifted relative to its forearc basin (Figure 4). Otherwise, to the north of the "E-W trending sheared zone" the Ryukyu crust should have sub-sided. Moreover, some earthquakes show south-dipping normal faulting above the frontal portion of the seismogenic zone (Figure 4), which is in opposition to a depression or subsidence to the north of the pro-posed tear fault.

The location of the updip limit generally marks the seaward aseismic sliding from the seismogenic zone (Hyndman et al., 1997) or a change from unconsolidated sediments to lithified rock (Byrne, 1998). Thus, the step-down may suggest that the seaward updip portion of the subducting sediments is "squeezed," peeled off, and partly accreted to the bottom of the forearc basin and arc (Figure 4). The group of aftershocks exists beneath the seismogenic zone thus implies that the occurrence of the 0420 event has accompanied under-plating. However, unlike the Naikai subduction zone where the underplating occurs beneath the accreted prism (Matsumura et al., 2003), the underplating in the southernmost Ryukyu subduction could begin at ~25 km deep beneath the forearc basin.

4.4. Exhumation of South Ryukyu Crust

There is a group of aftershocks appears above the frontal portion of the seismogenic zone (earthquakes inside circle c in Figure 3; Figure 4). This group is concentrated in the middle of group a and group b (Figure 3). Those aftershocks follow a trend dipping southward (Figure 4). Probably because the upper crust is relatively weak, the aftershocks of this group have shallow and small magnitudes less than 3 (Figure S4).

In fact, that shallow group extends from the southern slope of the Ryukyu Arc to the updip limit of the seis-mogenic zone (Figure 4). Based on the focal mechanisms found in this area (Theunissen et al., 2012), the shallow group of the 0420 aftershocks is probably associated with normal faulting (Figure 4). The normal faulting could be related to a set of normal faults in the east of Hoping Rise (Font et al., 2001; Figure 1). Furthermore, the lower crust of the Ryukyu Arc above the seismogenic zone is obviously arched (Figure 4). Thus, we may interpret the lower crust of the Ryukyu Arc above the seismogenic zone has been compressed and exhumed. It may explain why the Nanao forearc basin has a depressed space to receive lots of sediments. Because of spatial and temporal correlation, the underplating beneath the south Ryukyu Arc may have contributed to the exhumation of south Ryukyu Arc.

For the 0420 event, we may observe not only the occurrence of the aftershocks along the seismogenic zone, but also the underplating and the exhumation below and above the seimogenic zone, respectively. We have inspected the time series of the aftershocks, but we cannot find the temporal difference between the after-shocks associated with the underplating and the exhumation. Although the aftershocks were recorded 1 day after the 0420 main shock, we may attempt to conclude that the underplating and the exhumation are coseismic events. At least, the underplating and the exhumation occurred synchronously.

5. Conclusion

The seismogenic zone of the southernmost Ryukyu subduction zone is located beneath the rear part of the Nanao forearc basin and the frontal part of the Ryukyu Arc, at the plate interface from ~20 to 32 km deep. The width of the seismogenic zone is only ~35 km long. The southernmost Ryukyu seismogenic zone is very active and bounded by two main NW-SE trending dextral strike-slip fault zones. After analyzing the after-shocks of the 0420 event occurred in the southernmost Ryukyu seismogenic zone, we found that the after-shocks mainly occurred in the Nanao cluster and are distributed around the seismogenic zone of the subducting plate interface. Several tectonic structures have activated synchronously during the subducting

earthquake event in the southernmost Ryukyu subduction zone. (1) The dextral strike-slip NFZ and the SFZ have slipped, as evidenced by the dextral strike-slip components of focal mechanisms of the aftershocks around the NFZ and the SFZ. (2) A tectonic underplating has taken place beneath the southernmost Ryukyu seismogenic zone. (3) Probably due to the underplating beneath the seismogenic zone and/or the lateral compression on the overriding plate above the seismogenic zone, the lower crust of the Ryukyu Arc has exhumed and caused south-dipping normal faults near the boundary between the south Ryukyu arc and forearc basin.

References

Allen, R. V. (1978). Automatic earthquake recognition and timing from single traces. *Bulletin of the Seismological Society of America*, *68*(5), 1521–1532.

Almeida, R., Lindsey, E. O., Bradley, K., Hubbard, J., Mallick, R., & Hill, E. M. (2018). Can the updip limit of frictional locking on megathrusts be detected geodetically? Quantifying the effect of stress shadows on near-trench coupling. *Geophysical Research Letters*, *45*, 4754–4763. https://doi.org/10.1029/2018GL077785

Angelier, J. (1990). Geodynamic evolution of the eastern Eurasian margin. *Tectonophysics*, *123*, VII-X.

Byrne, T. (1998). Seismicity, slate belts and coupling along convergent plate boundaries. *Eos Transactions American Geophysical Union*, 79.

Chen, H. Y., Ikuta, R., Lin, C. H., Hsu, Y. J., Kohmi, T., Wang, C. C., et al. (2018). Back-arc opening in the western end of the Okinawa Trough revealed from GNSS/acoustic measurements. *Geophysical Research Letters*, *45*, 137–145. https://doi.org/10.1002/2017GL075724

Dominguez, S., Lallemand, S., Malavieille, J., & Schnürle, P. (1998). Oblique subduction of the Gagua Ridge beneath the Ryukyu accretionary wedge system: Insights from marine observations and sandbox experiments. *Marine Geophysical Researches*, *20*(5), 383–402. https://doi.org/10.1023/A:1004614506345

Font, Y., Liu, C. S., Schnurle, P., & Lallemand, S. (2001). Constraints on backstop geometry of the southwest Ryukyu subduction based on reflection seismic data. *Tectonophysics*, *333*(1–2), 135–158. https://doi.org/10.1016/S0040-1951(00)00272-9

Hayes, G. P., Wald, D. J., & Johnson, R. L. (2012). Slab1. 0: A three-dimensional model of global subduction zone geometries. *Journal of Geophysical Research*, *117*, B01302. https://doi.org/10.1029/2011JB008524

Herrendörfer, R., Van Dinther, Y., Gerya, T., & Dalguer, L. A. (2015). Earthquake supercycle in subduction zones controlled by the width of the seismogenic zone. *Nature Geoscience*, *8*(6), 471–474. https://doi.org/10.1038/ngeo2427

Heuret, A., Lallemand, S., Funiciello, F., Piromallo, C., & Faccenna, C. (2011). Physical characteristics of subduction interface type seismogenic zones revisited. *Geochemistry, Geophysics, Geosystems*, *12*, Q01004. https://doi.org/10.1029/2010GC003230

Ho, C. (1986). A synthesis of the geologic evolution of Taiwan. *Tectonophysics*, *125*(1–3), 1–16. https://doi.org/10.1016/0040-1951(86)90004-1

Hsu, S. K. (2001). Lithospheric structure, buoyancy and coupling across the southernmost Ryukyu subduction zone: An example of decreasing plate coupling. *Earth and Planetary Science Letters*, *186*(3–4), 471–478. https://doi.org/10.1016/S0012-821X(01)00261-8

Hsu, S. K., Liu, C. S., Shyu, C. T., Liu, S. Y., Sibuet, J. C., Lallemand, S., et al. (1998). New gravity and magnetic anomaly maps in the Taiwan-Luzon region and their preliminary interpretation. *Terrestrial Atmospheric and Oceanic Sciences*, *9*(3), 509–532.

Hsu, S. K., Sibuet, J. C., Monti, S., Shyu, C. T., & Liu, C. S. (1996). Transition between the Okinawa trough backarc extension and the Taiwan collision: New insights on the southernmost Ryukyu subduction zone. *Marine Geophysical Researches*, *18*(2–4), 163–187. https://doi.org/10.1007/BF00286076

Hsu, S. K., Sibuet, J. C., & Shyu, C. T. (2001). Magnetic inversion in the East China Sea and Okinawa Trough: Tectonic implications. *Tectonophysics*, *333*(1–2), 111–122. https://doi.org/10.1016/S0040-1951(00)00270-5

Hsu, Y. J., Simons, M., Avouac, J. P., Galetzka, J., Sieh, K., Chlieh, M., et al. (2006). Frictional afterslip following the 2005 Nias-Simeulue earthquake, Sumatra. *Science*, *312*(5782), 1921–1926. https://doi.org/10.1126/science.1126960

Hyndman, R. D. (2013). Downdip landward limit of Cascadia great earthquake rupture. *Journal of Geophysical Research: Solid Earth*, *118*, 5530–5549. https://doi.org/10.1002/jgrb.50390

Hyndman, R. D., Yamano, M., & Oleskevich, D. A. (1997). The seismogenic zone of subduction thrust faults. *Island Arc*, *6*(3), 244–260. https://doi.org/10.1111/j.1440-1738.1997.tb00175.x

Kao, H., Shen, S. S. J., & Ma, K. F. (1998). Transition from oblique subduction to collision: Earthquakes in the southernmost Ryukyu arc-Taiwan region. *Journal of Geophysical Research*, *103*(B4), 7211–7229. https://doi.org/10.1029/97JB03510

Kearey, P., Klepeis, K. A., & Vine, F. J. (2009). *Global tectonics* (3rd ed., Vol. 482). Oxford: Wiley-Blackwell.

Kennett, B. L. N., & Engdahl, E. R. (1991). Traveltimes for global earthquake location and phase identification. *Geophysical Journal International*, *105*(2), 429–465. https://doi.org/10.1111/j.1365-246X.1991.tb06724.x

Kimura, G., Kitamura, Y., Hashimoto, Y., Yamaguchi, A., Shibata, T., Ujiie, K., & Okamoto, S. Y. (2007). Transition of accretionary wedge structures around the up-dip limit of the seismogenic subduction zone. *Earth and Planetary Science Letters*, *255*(3–4), 471–484. https://doi.org/10.1016/j.epsl.2007.01.005

Kimura, G., & Ludden, J. (1995). Peeling oceanic crust in subduction zones. *Geology*, *23*(3), 217–220. https://doi.org/10.1130/0091-7613(1995)023<0217:POCISZ>2.3.CO;2

Kimura, H., Takeda, T., Obara, K., & Kasahara, K. (2010). Seismic evidence for active underplating below the megathrust earthquake zone in Japan. *Science*, *329*(5988), 210–212. https://doi.org/10.1126/science.1187115

Kinoshita, M., Araki, E., Kimura, T., Kopf, A., Saffer, D., & Toczko, S. (2017). Reconstruction of recent 10Ma thermal structure seaward of updip limit of Nankai seismogenic zone off Kumano inferred from IODP NanTroSEIZE geothermal data and time-dependent numerical model. In EGU General Assembly Conference Abstracts (Vol. 19, p. 10392).

Kissling, E., Kradolfer, U., & Maurer, H. (1995). *Program VELEST user's guide—Short introduction*. Switzerland: Institute of Geophysics, ETH Zurich.

Lallemand, S., Liu, C. S., Dominguez, S., Schnürle, P., & Malavieille, J. (1999). Trench-parallel stretching and folding of forearc basins and lateral migration of the accretionary wedge in the southern Ryukyus: A case of strain partition caused by oblique convergence. *Tectonics*, *18*(2), 231–247. https://doi.org/10.1029/1998TC900011

Lallemand, S., Theunissen, T., Schnürle, P., Lee, C. S., Liu, C. S., & Font, Y. (2013). Indentation of the Philippine Sea plate by the Eurasia plate in Taiwan: Details from recent marine seismological experiments. *Tectonophysics*, *594*, 60–79. https://doi.org/10.1016/j.tecto.2013.03.020

Lee, S.-J. (2015). Numerical earthquake model of the 20 April 2015 southern Ryukyu subduction zone M6. 4 event and its impact on seismic hazard assessment. *Earth, Planets and Space*, *67*(1), 164. https://doi.org/10.1186/s40623-015-0337-5

Matsumura, M., Hashimoto, Y., Kimura, G., Ohmori-Ikehara, K., Enjohji, M., & Ikesawa, E. (2003). Depth of oceanic-crust underplating in a subduction zone: Inferences from fluid-inclusion analyses of crack-seal veins. *Geology*, *31*(11), 1005–1008. https://doi.org/10.1130/G19885.1

Moore, J. C., & Saffer, D. (2001). Updip limit of the seismogenic zone beneath the accretionary prism of southwest Japan: An effect of diagenetic to low-grade metamorphic processes and increasing effective stress. *Geology*, *29*(2), 183–186. https://doi.org/10.1130/0091-7613(2001)029<0183:ULOTSZ>2.0.CO;2

Nishimura, S., Hashimoto, M., & Ando, M. (2004). A rigid block rotation model for the GPS derived velocity field along the Ryukyu arc. *Physics of the Earth and Planetary Interiors*, *142*(3–4), 185–203. https://doi.org/10.1016/j.pepi.2003.12.014

Paige, C., & Saunders, M. A. (1982). LSQR: Sparse linear equations and least squares problems, Part I and Part II. *ACM Transactions on Mathematical Software*, *8*, 43–71. https://doi.org/10.1145/355984.355989

Seno, T., Stein, S., & Gripp, A. E. (1993). A model for the motion of the Philippine Sea plate consistent with NUVEL-1 and geological data. *Journal of Geophysical Research*, *98*(B10), 17941–17948. https://doi.org/10.1029/93JB00782

Shin, T. C. (1993). The calculation of local magnitude from the simulated Wood-Anderson seismograms of the short-period seismograms in the Taiwan area. *Terrestrial Atmospheric and Oceanic Sciences*, *4*(2), 155–170.

Shin, T. C., Chang, C. H., Pu, H. C., Hsiao-Wei, L., & Leu, P. L. (2013). The geophysical database management system in Taiwan. *Terrestrial Atmospheric and Oceanic Sciences*, *24*(1), 11.

Sibuet, J. C., & Hsu, S. K. (2004). How was Taiwan created? *Tectonophysics*, *379*(1–4), 159–181. https://doi.org/10.1016/j.tecto.2003.10.022

Suppe, J. (1984). Kinematics of arc-continent collision, flipping of subduction, and back-arc spreading near Taiwan. *Memoir of Geological Society of China*, *6*(21), V33.

Teng, L. S. (1990). Geotectonic evolution of late Cenozoic arc-continent collision in Taiwan. *Tectonophysics*, *183*(1–4), 57–76. https://doi.org/10.1016/0040-1951(90)90188-E

Theunissen, T., Font, Y., Lallemand, S., & Liang, W. T. (2010). The largest instrumentally recorded earthquake in Taiwan: Revised location and magnitude, and tectonic significance of the 1920 event. *Geophysical Journal International*, *183*(3), 1119–1133. https://doi.org/10.1111/j.1365-246X.2010.04813.x

Theunissen, T., Lallemand, S., Font, Y., Gautier, S., Lee, C. S., Liang, W. T., et al. (2012). Crustal deformation at the southernmost part of the Ryukyu subduction (East Taiwan) as revealed by new marine seismic experiments. *Tectonophysics*, *578*, 10–30. https://doi.org/10.1016/j.tecto.2012.04.011

Waldhauser, F., & Ellsworth, W. L. (2000). A double-difference earthquake location algorithm: Method and application to the northern Hayward fault, California. *Bulletin of the Seismological Society of America*, *90*(6), 1353–1368. https://doi.org/10.1785/0120000006

Wang, K., & Hu, Y. (2006). Accretionary prisms in subduction earthquake cycles: The theory of dynamic Coulomb wedge. *Journal of Geophysical Research*, *111*, B06410. https://doi.org/10.1029/2005JB004094

Wang, T. K., Lin, S. F., Liu, C. S., & Wang, C. S. (2004). Crustal structure of the southernmost Ryukyu subduction zone: OBS, MCS and gravity modelling. *Geophysical Journal International*, *157*(1), 147–163. https://doi.org/10.1111/j.1365-246X.2004.02147.x

Yilmaz, Ö. (2001). *Seismic data analysis: Processing, inversion, and interpretation of seismic data*. Tulsa, OK: Society of Exploration Geophysicists. https://doi.org/10.1190/1.9781560801580

Yu, S. B., Chen, H. Y., & Kuo, L. C. (1997). Velocity field of GPS stations in the Taiwan area. *Tectonophysics*, *274*(1–3), 41–59. https://doi.org/10.1016/S0040-1951(96)00297-1